JOURNAL OF GEOPHYSICAL RESEARCH, VOL. 105, NO. D15, PAGES 19,891–19,903, AUGUST 16, 2000

Analysis of gas-aerosol partitioning in the Arctic: Comparison of size-resolved equilibrium model results with field data

A. M. Fridlind and M. Z. Jacobson

Department of Civil and Environmental Engineering, Stanford University, Stanford, California

V.-M. Kerminen and R. E. Hillamo

Air Quality Research, Finnish Meteorological Institute, Helsinki, Finland

V. Ricard and J.-L. Jaffrezo

Laboratoire de Glaciologie et Géophysique de l'Environnement, Domaine Universitaire, Saint Martin d'Hères, France

Abstract. Size-resolved aerosol mass and gas concentrations were measured during the European Arctic Aerosol Study (EAAS). A thermodynamic equilibrium model was applied to the data in order to (1) test whether gas-aerosol equilibrium appeared to be obtained by NH_3, HNO_3, HCl, HCOOH, and CH_3COOH, and (2) test the sensitivity of gas-aerosol equilibrium to several nonvolatile organic acids that were measured. Model results indicated that all submicrometer, accumulation-mode aerosols appeared to be near equilibrium with NH_3. Supermicrometer, coarse-mode aerosols of recent marine origin appeared to be out of equilibrium with HNO_3 and closer to equilibrium with HCl, while continentally influenced aerosols sometimes appeared to be near equilibrium with both HNO_3 and HCl. However, the observed gas-aerosol partitioning of HCOOH and CH_3COOH could not be explained by effective Henry's law partitioning, consistent with other studies. Nonvolatile organic acids measured were methanesulfonate, oxalate, succinate, and glutarate. Sensitivity tests indicated that methanesulfonate retained ~30% of NH_4^+ under marine conditions but had <3% impact on other species and under other conditions. Whereas oxalic acid was predicted to be ~15–30% dissociated in the aerosol solution, succinic and glutaric acids were predicted to be <10% dissociated, limiting their ability to influence gas-aerosol partitioning. Together, the three dicarboxylic acids were responsible for retaining 0–2% of predicted NH_4^+ and displacing 0–6% of predicted Cl^- and NO_3^-. Model results were sensitive to the assumed mixing state of the aerosols, as well as the degree of aerosol size resolution represented by the model.

1. Introduction

An important uncertainty in quantifying anthropogenic influences on global climate is associated with the direct and indirect effects of aerosols [*Intergovernmental Panel on Climate Change*, 1996]. To address this, recent research has been aimed at establishing the global geographic distribution and variability of aerosol characteristics. In the Arctic Basin, aerosols are influenced by unique regional processes, such as Arctic Haze during polar night [*Sirois and Barrie*, 1999], intense photochemistry at polar sunrise [*Kawamura et al.*, 1996], and low ammonia flux from local sources [*Bouwman et al.*, 1997]. However, few monitoring programs have studied aerosol chemistry and optical properties at high northern latitude sites. The European Arctic Aerosol Study (EAAS) was designed to measure the chemical and optical properties of aerosols in the Arctic troposphere and investigate their seasonal variability. Field measurements were made in northern Finland from July 1997 through July 1999, including continuous monitoring of aerosol number concentrations, chemical composition, and optical properties [*Virkkula et al.*, 1997]. Because gases influence aerosol chemistry, gas-aerosol partitioning was also studied during three intensive sampling campaigns. This paper focuses exclusively on the gas-aerosol partitioning behavior observed during the first intensive field campaign.

Few abundant atmospheric species are present at high concentrations in both the gas and aerosol phases. By contrast, most other species are concentrated predominantly in one phase. For example, SO_2 may be present at high concentrations in the gas phase, but does not dissolve significantly in aerosol solutions due to its relatively low Henry's constant. (While dissolved SO_2 may react irreversibly with oxidants such as H_2O_2(aq) to form other species, it does not significantly accumulate in an unreacted form.) At the opposite extreme, H_2SO_4 may be present at low concentrations in the gas phase, but accumulates significantly in aerosol solutions due to its very low volatility. Between these two extremes, a few species may partition in a more equal fashion. The abundant inorganic gases with high concentrations in the aerosol phase are ammonia (NH_3), hydrochloric acid (HCl), and nitric acid (HNO_3). Many organic gases may also partition significant mass to atmospheric aerosols, but few individual species have been quantified in both gas and aerosol phases. Of those, formic acid (HCOOH) and acetic acid (CH_3COOH) have exhibited among the highest concentrations in both phases [e.g., *Meng et al.*, 1995; *Saxena and Hildemann*, 1996]. During the EAAS intensive field campaigns all five gases (NH_3, HCl, HNO_3, HCOOH, and CH_3COOH) and their aerosol-phase analogs (as

Paper number 2000JD900257.
0148-0227/00/2000JD900257$09.00

water-soluble NH_4^+, Cl^-, NO_3^-, $HCOO^-$, and CH_3COO^-) were measured simultaneously. The aerosol sampling further aimed to characterize all nonvolatile inorganic species that may contribute significantly to water-soluble aerosol mass, thus in turn affecting gas-aerosol partitioning, as well as several nonvolatile organic species. Nonvolatile inorganics measured were the remaining dominant water-soluble constituents of sea salt, crustal matter, and secondary aerosols: Na^+, Mg^{2+}, Ca^{2+}, K^+, SO_4^{2-}, and $CH_3SO_3^-$ (methanesulfonate). Nonvolatile organics measured were three dicarboxylic acids that may be among the most concentrated organic aerosol species [*Saxena and Hildemann*, 1996]: $C_2O_4^{2-}$ (oxalate), $C_4H_4O_4^{2-}$ (succinate), and $C_5H_6O_4^{2-}$ (glutarate).

To analyze the observed gas-aerosol partitioning, a thermodynamic equilibrium model was applied. Previous modeling results have shown that gases and aerosols may be close to thermodynamic equilibrium at high relative humidities [*Jacobson*, 1997a]. However, large aerosols may require long time periods to equilibrate with some gases [*Meng and Seinfeld*, 1996]. Thermodynamic equilibrium models may be employed within the framework of a three-dimensional, time-dependent model in which equilibrium may be coupled with other processes, such as growth, gas chemistry, and sedimentation [e.g., *Jacobson*, 1997b, c; *Meng et al.*, 1998], or they may also be employed to calculate the instantaneous equilibrium of a gas-aerosol system [e.g., *Hildemann et al.*, 1984; *Hayami and Carmichael*, 1997, 1998; *Jacobson*, 1999a]. The latter approach was taken here, and the gas-aerosol equilibrium calculated by the model was compared with the observations. Similar applications of equilibrium models to size-distributed aerosol field data have been limited to the application of the SCAPE model to 2-stage particle impactor data collected in South Korea [*Hayami and Carmichael*, 1997, 1998] and the application of the EQUISOLV II model to 8-stage particle impactor data collected in the Los Angeles Basin [*Jacobson*, 1999a]. In this work, we applied EQUISOLV II to 12-stage particle impactor data that were inverted to estimate aerosol soluble mass concentration in 99 contiguous size bins. The specific goals of the modeling were (1) to test whether gas-aerosol equilibrium appeared to be obtained by both inorganic and organic partitioning species, and (2) to test the sensitivity of gas-aerosol equilibrium to the measured nonvolatile organic species. More generally, the model also tested whether the gas and aerosol observations fit together to form a physically consistent picture of size-resolved aerosol composition and gas-aerosol interaction.

In summary, the purpose of this paper is to present a modeling study of the gas-aerosol partitioning that was observed during the first EAAS intensive sampling campaign. We also report the subset of EAAS data that was used as model input. Future publications will be devoted to reporting the full range of data gathered during EAAS and studying the processes leading to the observed aerosol size distributions.

2. Experimental Data

The following provides a description of the field site, the methods used to sample aerosols and gases, the chemical analysis of aerosol and gas samples, and the inversion of particle impactor data to obtain near-continuous aerosol mass size distributions. All model input data are also reported.

2.1. Field Site

Field measurements were made at Sevettijarvi (69°35'N, 28°50'S, 130 m above sea level) in the Finnish Lapland (Figure 1). The site receives a wide variety of air masses. Easterly flow brings air masses influenced by Nickel/Zapolyarnyi, Russia, which is located 60 km from the station and is a primary source of SO_2 north of the Arctic Circle due to emissions from nonferrous metal production and coal- and oil-fired power plants [*Tuovinen et al.*, 1993]. Northerly and westerly flows bring air

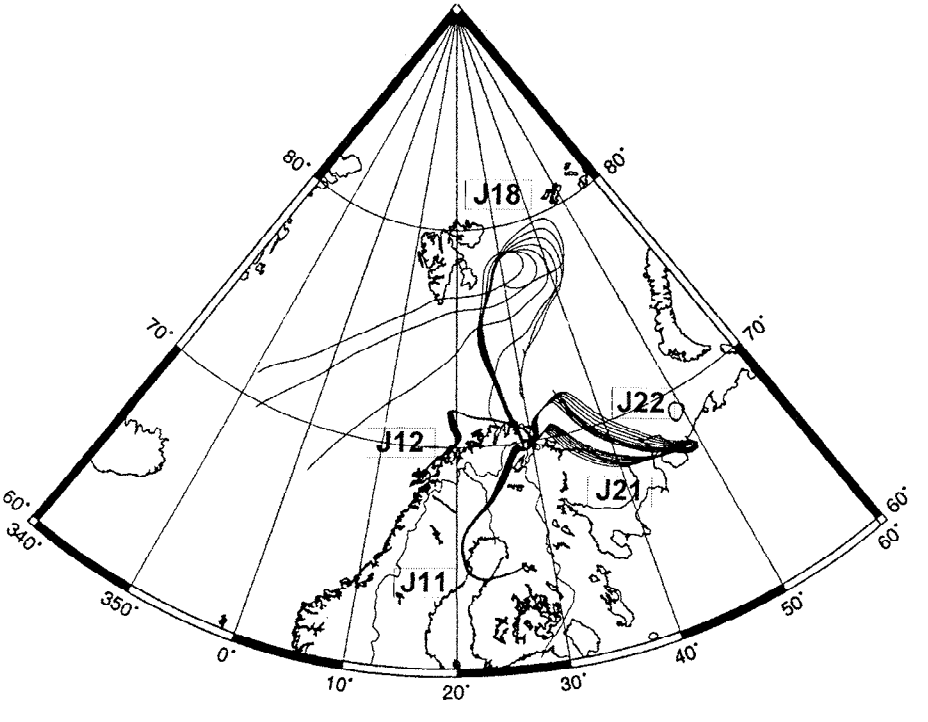

Figure 1. Four-day air mass trajectories for all aerosol samples modeled.

masses from the Barents Sea (the closest water body, located 40 km from the station), the Arctic Ocean, the Norwegian Sea, and the Gulf of Botnia. Southerly flow can bring polluted air masses from continental Europe [*Virkkula et al.*, 1997]. Local biogenic emissions from the boreal forest are also likely to influence aerosol characteristics, particularly during summer under anticyclonic conditions.

The sampling site is located on a small hill 50 m above the surrounding terrain, with sparse vegetation, mainly pine and birch trees. Local contamination sources are limited to several houses within 3 km, and there is no major population center within 30 km of the station. The closest road is 3 km away, with traffic limited to a few vehicles per day. The station consists of two log cabins. One cabin houses the pumps for aerosol and gas sampling, with filtered exhausts. The second cabin houses the sampling equipment, with inlets extending to a deck 7 m above ground level [*Virkkula et al.*, 1997].

In this paper, we report a subset of the data gathered during late July of 1997. The data include size-resolved aerosol mass and gas concentrations, as described below. Additional measurements were 1-hour average particle number concentrations at 7 m above ground level and 5-min average temperature, relative humidity, and atmospheric pressure at 2 m above ground level [*Virkkula et al.*, 1995, 1997].

2.2. Aerosol Sampling

A 12-stage Small Deposit-Area Impactor (SDI) designed at the Finnish Meteorological Institute was used to sample aerosols with mean diameters ranging from 45 nm to 15 μm [*Maenhaut et al.*, 1996; *Kerminen et al.*, 1998a]. Aerosols were sampled 7 m above ground level at ambient temperature and relative humidity, with a flow rate of 10.8 L min^{-1} (STP). Typical sampling periods lasted 12 hours, during either daytime (0900–2100) or nighttime (2100–0900). Nucleopore film was used as the impaction substrate and was coated with Apiezon L grease in order to limit particle bounce. Under a laminar flow hood, impactors were loaded immediately prior to sampling and downloaded immediately after collection. Samples were individually extracted in test tubes with 5 mL of Milli-Q water within 15 min of collection in order to limit exchange with the gas phase during storage. Impactor substrate blanks were prepared and treated in the same manner as samples, including grease coating, but were not loaded into the impactor. One pair of blanks was analyzed for each aerosol sampling period.

Potential sampling artifacts were considered negligible. Impactor sampling of semivolatile species is less prone to artifacts than filter sampling, and NO_3^- loss from impactors has been shown to be low when the particulate fraction exceeds 0.5 [*Zhang and McMurry*, 1992], as was the case during EAAS. Losses due to pressure changes within the impactor are further limited to the stages collecting the smallest particles. However, particles of 0.2 μm diameter were still collected at 95% of atmospheric pressure in the SDI [*Maenhaut et al.*, 1996]. Data and modeling also indicated that NO_3^- was not present in semivolatile forms such as NH_4NO_3(s) in the samples reported here.

2.3. Gas Sampling

All gases were sampled using a modified version of the mist chamber technique [*Talbot et al.*, 1997; *Lefer et al.*, 1999], in which soluble gases are concentrated by exchange with a mist of water created in a sampling vessel. Two mist chambers working at a flow rate of 26 L min^{-1} (STP) were set in series in order to calculate the collection efficiencies for the chemical species. A Teflon filter (1.0 μm porosity, Millipore FA, Bedford, Massachusetts) was inserted in front of the first mist chamber to remove particles from the airstream. The filter can create positive interferences by volatilization from collected particles or negative interferences by gas adsorption, but these interferences were considered minimal under the conditions of sampling (low loading of the front filter and low concentrations of semivolatile NH_4NO_3(s) or basic coarse particles) [*Lefer et al.*, 1999]. However, in order to further reduce possible interferences, the sampling intake was located downstream of a particle separator made of stainless steel tubing (75 mm diameter) connected to a high-volume pump with a flow rate of 1500 L min^{-1}. Laboratory tests indicated that essentially no particles larger than 0.7 μm entered the mist chamber intake at the prescribed flow rates [*Voisin et al.*, 2000].

Gases were sampled 1.5 m above ground level at ambient temperature, with sampling durations of 2 hours. The mist chambers were loaded with 20 mL of Milli-Q water and a new prefilter for each run. After collection, samples were stored at room temperature in cleaned, airtight glass bottles and analyzed in the field within 6 hours. Procedural blanks were performed several times per day and were treated in the same manner as samples. The season-averaged blank value was subtracted from sample values to calculate atmospheric concentrations.

2.4. Aerosol and Gas Sample Analysis

The impactor and mist chamber samples were analyzed in the field for cations and anions using ion chromatography. Cations (NH_4^+, Na^+, Mg^{2+}, Ca^{2+}, and K^+) were analyzed with a Dionex 100 chromatograph with a CS12 column and isocratic 96-m*M* methanesulfonic acid eluent, as prescribed by Dionex (Sunnyvale, California). Using a 700-μL injection loop gave sub-ppb detection limits for all cations in solution. Anions (Cl^-, NO_3^-, SO_4^{2-}, $CH_3SO_3^-$, $HCOO^-$, CH_3COO^-, $C_2O_4^{2-}$, $C_4H_4O_4^{2-}$, and $C_5H_6O_4^{2-}$) were analyzed with a Dionex 500 chromatograph with an AS11 column, as described by *Jaffrezo et al.* [1998]. Using a 500-μL injection loop gave sub-ppb detection limits for all anions in solution.

Table 1 gives the atmospheric detection limits for typical mist chamber samples, calculated as the average plus twice the standard deviation of all 40 procedural blanks that were collected. The detection limits were at least an order of magnitude lower

Table 1. Atmospheric Detection Limits (DL) of Gases and Aerosol Species (Single Impactor Stage)

Gases	DL, ng m^{-3}	Aerosol Species	DL, ng m^{-3}
HCl	1.5	NH_4^+	1.5
HNO_3	0.3	Na^+	9.4
NH_3	0.9	Mg^{2+}	3.8
formic acid	5.9	Ca^{2+}	4.5
acetic acid	4.1	K^+	2.7
		Cl^-	5.8
		NO_3^-	2.5
		SO_4^{2-}	8.3
		$CH_3SO_3^-$	2.6
		formate	25.3
		acetate	11.9
		oxalate	1.4
		succinate	0.8
		glutarate	0.5

Table 2. Sampling Duration (Local Time), Meteorological Conditions (Average and Standard Deviation), and Type of Aerosol Samples Modeled

Sample	Start Time	Stop Time	Temperature, °C	RH, %	Pressure, mbar	Aerosol Type
J11	July 17 2115	July 18 0900	17±1	80±6	1006±0.5	continental
J12	July 18 2200	July 19 0900	11±1	95±2	1008±0.6	continental
J18	July 25 1140	July 25 2110	8±1	68±2	1001±0.3	marine
J21	July 29 2145	July 30 0920	11±1	87±4	997±0.4	continental/marine
J22	July 30 2155	July 31 0925	8±1	92±3	1001±0.3	continental

than atmospheric concentrations of all gases except NH_3. Table 1 also gives atmospheric detection limits for a single stage of a typical particle impactor sample, calculated as the average plus twice the standard deviation of all 33 procedural blanks that were collected. However, inversion of the raw impactor data required concentrations above the detection limit on at least 3–4 stages. Thus, in practice, the atmospheric detection limits for aerosol species were 3–4 times those shown in Table 1. Concentrations of NH_4^+ and SO_4^{2-} were at least 5 times above the detection limits for all impactor samples. This was not always the case for the other major aerosol species (Na^+, Cl^-, and NO_3^-), and rarely the case for most minor species (Mg^{2+}, Ca^{2+}, K^+, and organics). Analytical difficulties precluded determination of Mg^{2+} in most samples.

Out of the 25 aerosol impactor samples collected during the summer campaign, 11 included both gas and aerosol concentrations for all major chemical species. Of these 11 complete samples, 5 were most suitable for modeling due to greater uniformity of observed particle number concentrations, gas concentrations, and relative humidity during the aerosol sampling period. The aerosol type for each of the 5 samples modeled (Table 2) was loosely defined according to the total observed Na^+: >350 ng m^{-3} was considered marine, 100–350 ng m^{-3} was considered continental/marine, and <100 ng m^{-3} was considered continental. The observed aerosol mass concentrations (Table 3) varied with aerosol type, but were within the range previously measured at the site [*Kerminen et al.*, 1999; *Virkkula et al.*, 1999]. While the aerosol type was often correlated with air mass trajectories (Figure 1), the correlation was sometimes weak. Trajectories indicated that some continental samples may have spent considerable time over the ocean, but provided no further information on the thermodynamic or elevation history of the aerosols.

The average and standard deviation of gas concentrations observed during each aerosol sampling period (Table 4) were calculated from the 2-hour mist chamber samples. Few comparable data exist for background concentrations at high latitudes. The values observed during EAAS were generally a factor of 3–5 higher for HCOOH and CH_3COOH than those presented by *Talbot et al.* [1992], and a factor of 2–3 lower for HNO_3. The extensive additional gas data collected during EAAS will be reported in a future publication.

2.5. Aerosol Impactor Data Inversion

The 12-stage particle impactor data were processed with the MICRON inversion routine [*Wolfenbarger and Seinfeld*, 1990] to obtain near-continuous aerosol mass size distributions with 99 size bins between 40 nm and 20 μm. The shape of the inverted size distribution obtained by MICRON depends not only on the impactor data but also on the overall uncertainty related to aerosol sampling, chemical analysis, and impactor collection efficiency. The detailed impactor efficiency data required by MICRON were taken from calibrations made at the Finnish Meteorological Institute [*Maenhaut et al.*, 1996]. Higher overall uncertainties typically lead to smoother inverted size distributions, while lower uncertainties reveal detailed structure in the distributions. Since it is difficult to precisely estimate the overall uncertainty, the sensitivity of the inverted size distributions to the magnitude of the uncertainty was tested. It was found that variations on the order of the experimental uncertainty in the input data sometimes produced two types of instability: (1) a large change in the amplitude of the minimum between overlapping modes (Figure 2a), and (2) a change in the total number of modes (Figure 2b). The first type of instability occurred only in sample J12 (for Na^+, Cl^-, and NO_3^-), whereas the second type occurred only in samples J21 and J22 (for SO_4^{2-} and/or NH_4^+).

The inverted aerosol mass size distributions of the major species that were used as model input (Figure 3) are in agreement with previous observations at the site [*Kerminen et al.*, 1999]. The experimental uncertainty in the inverted size distributions was obtained by simultaneously varying the raw impactor data over the range of experimental uncertainties for each stage. The inversion results are referred to hereafter simply as observations, with the understanding that they represent observations that have been processed by the MICRON routine.

Table 3. Observed Aerosol Mass Concentrations Summed Over Particle Impactor Stages

Sample	NH_4^+	Na^+	Mg^{2+}	Cl^-	NO_3^-	SO_4^{2}	CH_3SO_3	Formate	Acetate	Oxalate	Succinate	Glutarate
J11	238.5	<DL	NA	<DL	<DL	677.2	6.5	164.5	82.4	94.9	74.3	29.5
J12	224.4	45.4	<DL	31.6	28.1	802.2	167.9	79.0	63.7	106.7	45.3	13.7
J18	33.4	772.6	70.6	957.1	72.0	186.8	98.1	<DL	<DL	11.0	<DL	<DL
J21	227.6	272.5	34.9	207.5	174.5	789.8	46.2	<DL	<DL	50.5	48.6	16.2
J22	161.4	84.6	NA	71.1	56.0	1127.6	79.1	<DL	<DL	50.9	57.3	19.1

Units are ng m^{-3}; DL, detection limit; NA, not analyzed. Ca^{2+} and K^+ were below detection limits in all samples.

Table 4. Average and Standard Deviation of Gas Concentrations Observed During Each Aerosol Sampling Period

Sample	HCl	HNO_3	NH_3	HCOOH	CH_3COOH
J11	80±56	50±18	59.5±20.9	2898±662	2953±644
J12	52±18	17±9	6.2±7.2	1134±507	1044±459
J18	109±26	38±15	<DL	393±190	432±255
J21	86±15	15±5	1.6±1.0	1299±310	1615±594
J22	76±34	45±12	<DL	995±365	1064±493

Units are ng m^{-3}; DL, detection limit.

3. Gas-Aerosol Equilibrium Model

A thermodynamic equilibrium model was applied to the gas and aerosol observations. In the following, the model is described, and the model assumptions are discussed and evaluated.

3.1. Model Description

The EQUISOLV II model was used to calculate thermodynamic equilibrium among the gas-phase and size-resolved aerosol-phase species listed in Table 5. All thermodynamic data used by the model have been previously referenced [*Jacobson*, 1999a, b], with the exception of the data for aerosol organics that are referenced in section 4. Aerosol-phase inputs to the model were the observed size distributions of water-soluble NH_4^+, Na^+, Mg^{2+}, Cl^-, NO_3^-, SO_4^{2-}, $CH_3SO_3^-$, $HCOO^-$, CH_3COO^-, and in some cases oxalate, succinate, and glutarate, with charge imbalances attributed to unmeasured H^+ and CO_3^{2-}, in each of 99 size bins between 40 nm and 20 μm. Gas-phase inputs were estimated CO_2 and observed HCl, HNO_3, NH_3, HCOOH, and CH_3COOH.

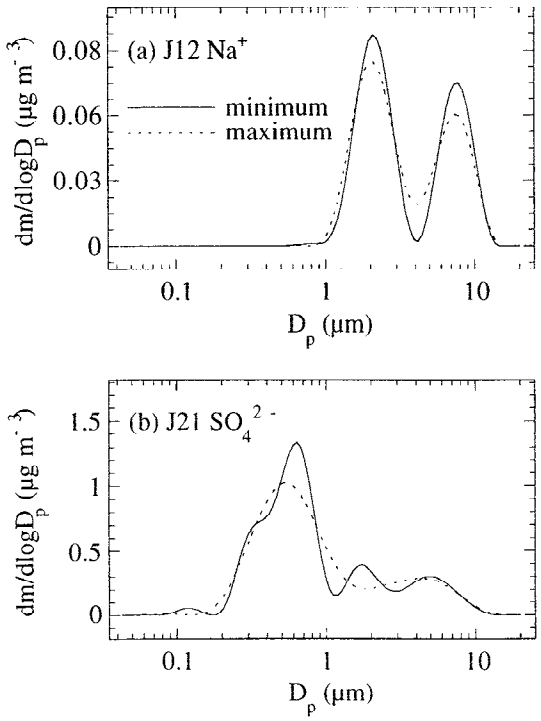

Figure 2. Examples of the inverted aerosol mass size distributions when the estimated minimum and maximum values of overall uncertainty were input to MICRON for (a) Na^+ in sample J12 and (b) SO_4^{2-} in sample J21.

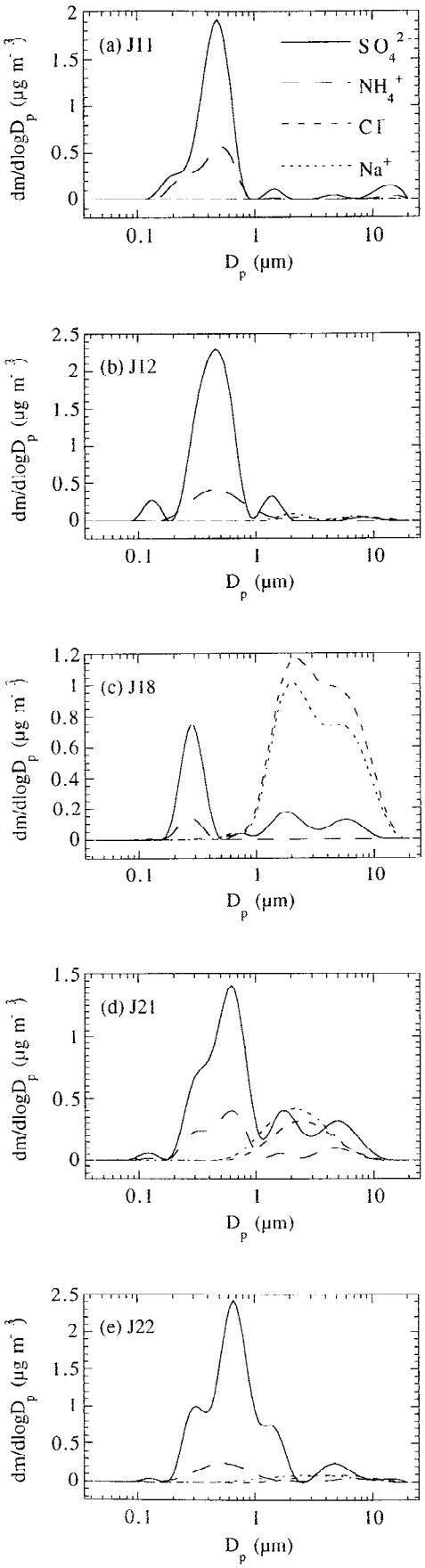

Figure 3. Inverted size distributions of SO_4^{2-}, NH_4^+, Cl^-, and Na^+ for all aerosol samples modeled.

Table 5. Gas-Phase and Aerosol-Phase Species (Aqueous, Ionic, and Solid) Included in EQUISOLV II

Gas	Aqueous	Ionic	Solid
H_2O	H_2O(aq)	H^+	NH_4NO_3(s)
CO_2	H_2CO_3(aq)	OH^-	NH_4Cl(s)
HCl	H_2SO_4(aq)	HCO_3^-	NH_4HSO_4(s)
HNO_3	CH_3SO_3H(aq)	CO_3^{2-}	$(NH_4)_2SO_4$(s)
NH_3	HCOOH(aq)	NH_4^+	$(NH_4)_3H(SO_4)_2$(s)
HCOOH	CH_3COOH(aq)	Na^+	NH_4HCO_3(s)
CH_3COOH	$C_2H_2O_4$(aq)	Mg^{2+}	$NaNO_3$(s)
	$C_4H_6O_4$(aq)	Cl^-	NaCl(s)
	$C_5H_8O_4$(aq)	NO_3^-	$NaHSO_4$(s)
		HSO_4^-	Na_2SO_4(s)
		SO_4^{2-}	$NaHCO_3$(s)
		$CH_3SO_3^-$	Na_2CO_3(s)
		$HCOO^-$	$MgCl_2$(s)
		CH_3COO^-	$Mg(NO_3)_2$(s)
		$C_2HO_4^-$	$MgSO_4$(s)
		$C_2O_4^{2-}$	$MgCO_3$(s)
		$C_4H_5O_4^-$	
		$C_4H_4O_4^{2-}$	
		$C_5H_7O_4^-$	
		$C_5H_6O_4^{2-}$	

An initial ambient CO_2 concentration of 360 ppm was assumed for all samples. Meteorological inputs were observed temperature, relative humidity, and pressure. Observed meteorological variables and gas concentrations were averaged over the aerosol sampling period (Tables 2 and 4).

During each model simulation all volatile species were permitted to simultaneously migrate between the gas phase and the aerosol size bins until thermodynamic equilibrium was established. Conceptually, this solution resolved the competitive thermodynamic demand of the nonvolatile species in each aerosol size bin for the total volatile species in the gas-aerosol system. Outputs of the model included the equilibrium concentration of all gases and the equilibrium size distribution of all aerosol species (Table 5).

The equilibrium solutions were both unique and converged for all model runs. The solutions were unique since no solids containing more than a single volatile component, such as NH_4HCO_3(s) or NH_4NO_3(s), were predicted [*Jacobson*, 1999a]. When such solids are predicted, their size-resolved distribution is not thermodynamically unique and would instead be governed by kinetic transport processes [*Wexler and Seinfeld*, 1990]. For this study, all solids were assumed to form at their crystallization relative humidity, and none were predicted in the samples modeled. Convergence was confirmed by comparing each solution with that obtained when all inorganic volatile species (NH_4^+, Cl^-, and NO_3^-) were removed to the gas phase (added to observed NH_3, HCl, and HNO_3). Since the system always had a unique solution, such drastic alteration of the initial conditions of the volatile species did not change the converged solution. All solutions met two criteria to guarantee the convergence of both aerosol size-distributions and overall gas-aerosol partitioning: (1) the predictions of inorganic volatile species in each size bin containing more than 1% of total volatile mass differed from one another by less than 1%, and (2) their sum over all size bins differed from one another by less than 0.5%.

Model results are shown only for volatile species since nonvolatile species were unable to migrate from their initial size bins and their water-soluble concentrations therefore did not deviate from the initialized values. Model results are presented below in three forms: (1) the aerosol mass size distribution; (2) the total aerosol mass concentration, obtained by summing over all size bins; and (3) the total aerosol mass concentration relative to the combined mass in the aerosol and gas phases, referred to as the particulate fraction. Deviations between model predictions and observations would result from three general sources: (1) error in the model representation of the gas-aerosol system, (2) error in observations, or (3) lack of thermodynamic equilibrium in the observed system.

3.2. Model Assumptions and Uncertainty

In addition to assuming gas-aerosol equilibrium, it was assumed that all species that affect gas-aerosol equilibrium were included in the model. The EAAS study was designed to satisfy this assumption, as discussed in section 1. Specific additional assumptions regarding gases, meteorological conditions, and aerosols were tested in order to evaluate model uncertainty, as described in the following.

3.2.1. Gases and meteorological conditions. Multistage particle impactors require significant sampling duration to accumulate sufficient aerosol mass for chemical analysis. During EAAS, gas concentrations and meteorological conditions sometimes varied widely over the 12 hours required to obtain each aerosol sample, and these variations were generally much greater than experimental uncertainty in the measured variables (Tables 2 and 4). The sensitivity of the results to the observed variations were evaluated as follows: (1) each gas concentration was independently initialized to its minimum and maximum observed values, (2) all meteorological variables (temperature, relative humidity, and pressure) were simultaneously initialized to their observed values at points of minimum and maximum relative humidity, and (3) all gas concentrations and meteorological variables were simultaneously initialized to their values at points of minimum and maximum relative humidity. The results of these sensitivity tests are presented in Table 6 in terms of changes in total predicted NH_4^+, Cl^-, and NO_3^- in the aerosol phase, summed over all size bins.

Independent variations in gas concentrations influenced predictions by up to ±23%. Whereas changing NH_3 only influenced NH_4^+, HCl and HNO_3 exhibited competitive displacement in the aerosol phase. The independent behavior of NH_3 can be attributed to the association of NH_3 with the accumulation mode, whereas HCl and HNO_3 were interdependently associated with the coarse mode.

Variations in meteorological conditions influenced predictions by up to ±16%. Meteorological conditions at maximum relative humidity generally increased predicted aerosol absorption of NH_3 and HCl due to increased water content. By contrast, HNO_3 absorption was decreased due to the increased dissolution of HCl and subsequent lowering of pH. The opposite effects occurred at minimum relative humidity.

Simultaneous variations in gas concentrations and meteorological conditions influenced predictions by up to ±20%. Relative humidity was maximum during early morning, when gas concentrations were generally lowest, and the opposite was generally true in early afternoon, often resulting in competing equilibrium effects. Thus, for instance, high NH_3 tended to increase equilibrium NH_4^+, while simultaneously low relative humidity tended to decrease it. However, the dominant effect varied among both samples and gases.

3.2.2. Aerosols. The aerosol population was assumed to be constant over the 12-hour sampling period. Since number con-

Table 6. Percentage Change of Total NH_4^+, Cl^-, and NO_3^- (Summed Over All Size Bins) Predicted by Each Sensitivity Test

	ΔNH_4^+					ΔCl^-					ΔNO_3^-				
Sensitivity Test	J11	J12	J18	J21	J22	J11	J12	J18	J21	J22	J11	J12	J18	J21	J22
Gas concentrations															
NH_3 minimum	-3	-3	—	0	—	—	0	—	0	—	—	0	—	0	—
NH_3 maximum	3	5	—	0	—	—	1	—	0	—	—	0	—	0	—
HCl minimum	0	0	0	0	0	—	-15	-2	-2	-11	—	23	0	2	14
HCl maximum	0	0	0	1	0	—	6	4	7	13	—	-8	0	-11	-17
HNO_3 minimum	0	0	0	0	0	—	4	0	2	6	—	-8	-8	-4	-9
HNO_3 maximum	0	0	0	0	0	—	-5	0	-9	-6	—	8	11	19	9
Meteorological conditions															
at RH minimum	-6	-1	0	-6	0	—	-7	0	-3	-13	—	8	0	4	14
at RH maximum	4	0	0	4	0	—	3	0	4	16	—	-1	0	-1	-4
Combined gas and meteorological															
at RH minimum	-3	4	0	-6	0	—	-7	-2	-8	-8	—	8	-8	13	7
at RH maximum	1	-1	0	4	0	—	-9	4	4	-3	—	14	11	-3	20
Aerosol experimental uncertainty															
SO_4^{2-} minimum	-10	-1	-2	-8	0	—	18	0	6	17	—	13	0	3	15
SO_4^{2-} maximum	8	1	1	6	0	—	-21	0	-6	-8	—	-17	0	-3	-7
Na^+ minimum	—	0	1	3	0	—	-53	0	-11	-39	—	-48	0	-6	-37
Na^+ maximum	—	0	-1	-3	0	—	52	0	12	58	—	38	0	6	48
Model representation of size bins															
externally mixed (all size bins)	—	0	-1	22	0	—	35	0	44	320	—	26	0	18	200
one size bin only (internally mixed)	0	-1	-100	-64	0	—	-96	0	-87	-98	—	-94	0	-75	-98
two size bins only (internally mixed)	0	-1	-12	-1	0	—	-57	0	-3	-98	—	-48	0	-1	-98
Presence of organic acids															
without $CH_3SO_3^-$	0	-2	-27	-3	0	—	1	0	2	2	—	1	0	1	1
with dicarboxylic acids	2	0	0	0	0	—	-2	0	-1	-6	—	-2	0	0	-4

No value shown when concentrations of gas or aerosol species were below detection limits.

centration was observed with higher frequency, it was used as an indicator of the behavior of the population during each sample. The samples with the smallest changes in 1-hour average particle number concentration in the 0.3–0.5 μm size range were chosen for modeling in order to satisfy this assumption as nearly as possible (see section 2.4).

The aerosol population was assumed to be vertically constant between 7 m (the height of aerosol measurements) and 1.5–2 m (the height of gas and meteorological measurements). Profiles of NH_4^+, NO_3^-, Cl^-, Na^+, and SO_4^{2-} measured over land suggest that aerosol mass may vary by less than several percent over this elevation change [*Erisman et al.*, 1988], supporting the general validity of this assumption.

Aerosols were also assumed to be internally mixed in each size bin since particle impactors provide no data on aerosol mixing state on each stage. The influence of this assumption on model results was tested by assuming that the aerosol population was instead composed of two separate types of particles: (1) modified sea salts and (2) organic-enriched ammonium sulfates. The modified sea salts were assumed to be composed of observed Na^+, Cl^-, Mg^{2+}, sea-salt SO_4^{2-}, and NO_3^-, where sea-salt SO_4^{2-} was calculated from observed Na^+ using the standard composition of seawater [*Stumm and Morgan*, 1996]. The organic-enriched ammonium sulfates were assumed to be composed of the remaining observed mass, including NH_4^+, non-sea-salt SO_4^{2-}, $CH_3SO_3^-$, formate, and acetate. Each of the 99 size bins was thus separated into two size bins representing the two particle types, giving a total of 198 size bins, two of each size. It was not possible to perform this test for sample J11 since all primary sea salts were below detection limits.

Assumed mixing state influenced predictions for continentally influenced samples by up to ±320%, but influenced predictions for the marine sample by no more than 1% (Table 6). When non-sea-salt sulfates were separate from the sea salts, they retained NH_4^+ in the aerosol phase; when they were mixed with sea salts, they displaced Cl^- and NO_3^-. Thus the assumed degree of external mixture had a significant impact on the predicted gas-aerosol partitioning when sulfates were concentrated in the same particle size range as sea salts, as occurred to the greatest degree in the continentally influenced samples (see Figure 3). While it is likely that the actual (and unknown) degree of internal mixture affected the observed gas-aerosol partitioning to some degree since all particles in a given size range are not likely to be perfectly identical, it is impossible to evaluate the importance of this effect without further data on the actual mixing state of the aerosols.

As an aside, to briefly address the potential importance of aerosol size resolution in future modeling work, the sensitivity of the results to assuming (1) a single aerosol size bin, and (2) two aerosol size bins was also tested (Table 6). One size bin resulted in the acidic accumulation-mode aerosols being mixed with the less acidic coarse-mode aerosols (see Figure 3). Overall, Cl^- and NO_3^- were displaced by the increased acidity of the mixture relative to the coarse mode, whereas NH_4^+ was displaced by the decreased acidity of the mixture relative to the accumulation mode. Thus a one-bin model gave a poor representation of the thermodynamic gas-aerosol equilibrium in all samples except J11, which was composed only of ammonium sulfates. A two-bin model with bins separated at 1 μm gave similarly poor results in some samples (J12 and J22), but also gave more adequate representation of the 99-bin results in other samples (J11, J18, and J21) since it captured the primary chemical distinction between accumulation and coarse modes.

3.2.3. Experimental uncertainty. The experimental uncertainty in the inverted size distributions of the aerosol species was calculated as described in section 2.5. The uncertainty in the primary nonvolatile species, SO_4^{2-} and Na^+, influenced model results most, up to ±58% (Table 6). Further, model results were generally more sensitive to experimental uncertainty in the aero-

sol mass size distributions than to any other source of model uncertainty tested above, with the possible exception of mixing state, which could not be constrained. Specifically, NH_4^+ was generally most sensitive to the uncertainty in SO_4^{2-}, whereas Cl^- and NO_3^- were generally most sensitive to the uncertainty in Na^+. Thus these sensitivity tests were used to represent the effect of experimental uncertainty on model results.

4. Results

The model results were first compared with observations in order to evaluate whether gas-aerosol equilibrium may have been observed during EAAS (Figures 4–9). The sensitivity of the model results to the presence of organic acids was then analyzed in order to evaluate their potential influence on the gas-aerosol partitioning of the inorganic species.

4.1. Gas-Aerosol Partitioning

The observed size-resolved gas-aerosol partitioning of NH_3/NH_4^+, HCl/Cl^-, HNO_3/NO_3^-, $HCOOH/HCOO^-$, and CH_3COOH/CH_3COO^- was compared with the modeled equilibrium condition, and the results are discussed sequentially by species in the following. It is noted that minor discontinuities occurred in the results in several cases but were not important to overall conclusions. Discontinuities at ~0.2 μm and ~1 μm in sample J12 (Figures 5a–5c) resulted from charge imbalances due to differences in the inverted size distributions of NH_4^+ and SO_4^{2-} (Figure 3b). Discontinuities at ~2 μm in sample J22 (Figures 9b and 9c) resulted from discontinuities in sea-salt SO_4^{2-} when the inverted size distribution indicated that no SO_4^{2-} was present despite the presence of Na^+ (Figure 3e).

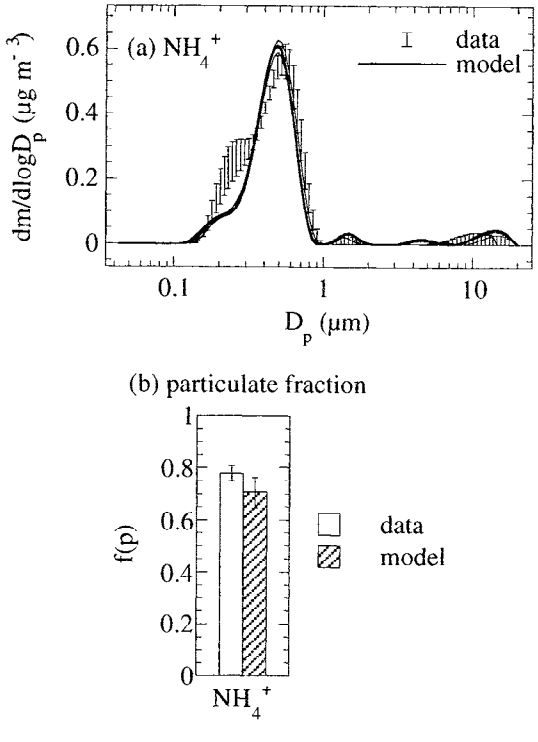

Figure 4. Sample J11 observations versus model results: (a) the aerosol mass size distribution of NH_4^+ and (b) the particulate fraction of NH_4^+. (Cl^- and NO_3^- were below detection limits.) Data shown in Figures 4a and 4b with error bars indicating the range of experimental uncertainty. Model results shown in Figure 4a as a heavy line and in Figure 4b as a shaded column, with the effect of experimental uncertainty (see section 3.2.3) shown in Figure 4a as thin lines and in Figure 4b as error bars.

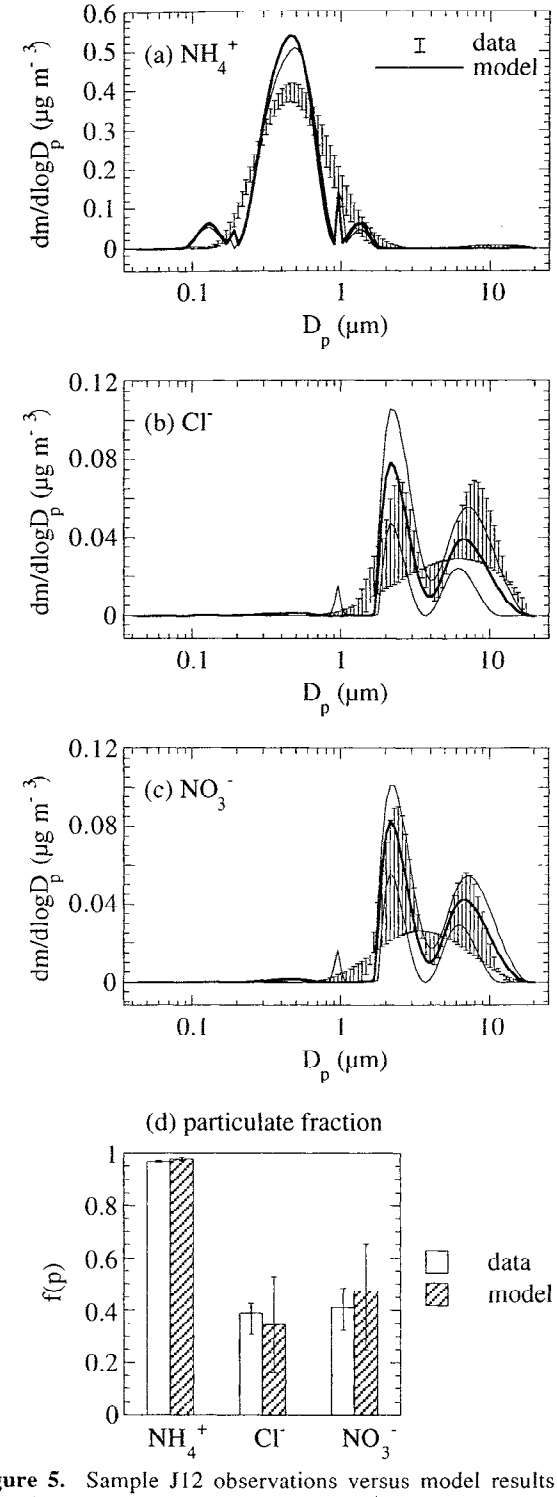

Figure 5. Sample J12 observations versus model results: the aerosol mass size distributions of (a) NH_4^+, (b) Cl^-, and (c) NO_3^-, and (d) the particulate fraction of all three species. Data shown in Figures 5a–5d with error bars indicating the range of experimental uncertainty. Model results shown in Figures 5a–5c as a heavy line and in Figure 5d as shaded columns, with the effect of experimental uncertainty (see section 3.2.3) shown in Figures 5a–5c as thin lines and in Figure 5d as error bars.

4.1.1. NH_3/NH_4^+. The predicted equilibrium mass size distribution and particulate fraction of NH_4^+ were fully within experimental uncertainty in the marine sample (Figures 6a and 6d).

This result is consistent with the hypothesis that the accumulation-mode aerosols were in equilibrium with NH_3 and were accurately represented by the model. The predicted particulate fraction of NH_4^+ was also within experimental uncertainty in three of the four remaining samples (Figures 4d, 5d, and 8d), but the predicted size distribution deviated outside the limits of experimental uncertainty in at least some size ranges in those samples (Figures 4a, 5a, and 8a). In the remaining sample, NH_4^+ was adequately predicted in the accumulation mode but drastically underpredicted in the coarse mode (Figure 7a), and the particulate fraction was also consequently underpredicted (Figure 7d). Generalizing these results, it appeared that most accumulation-mode aerosols were at or near equilibrium with NH_3, but predictions deviated from observations in the coarse mode when NH_4^+ was observed in that mode.

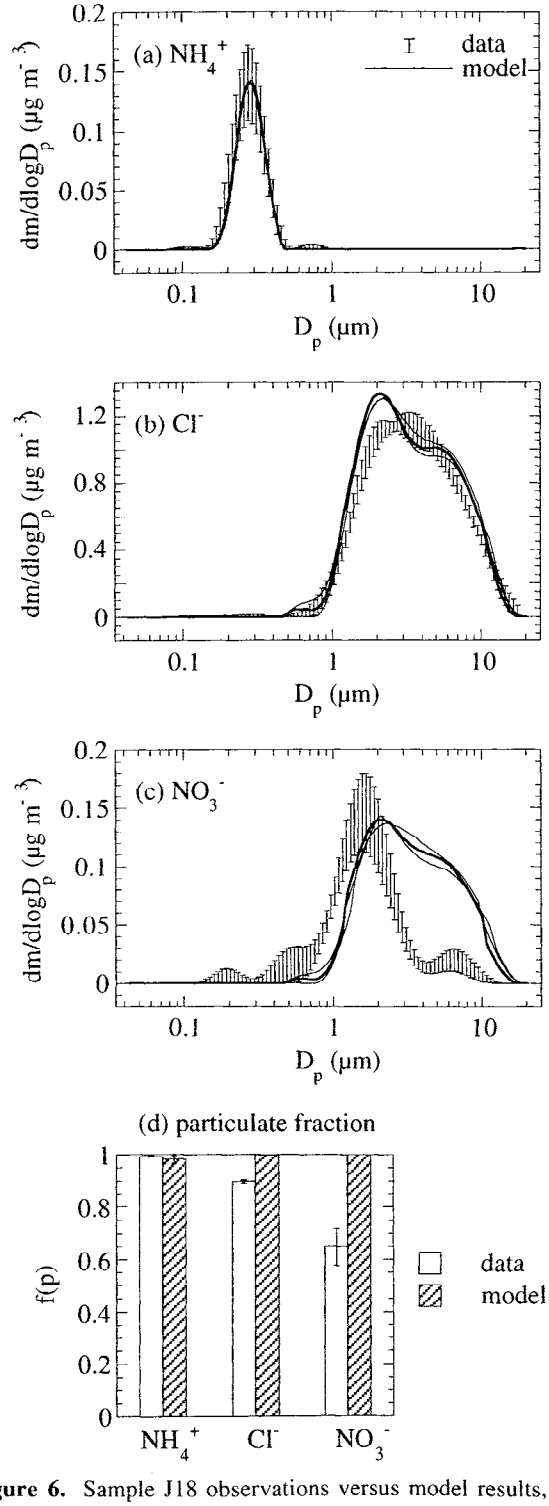

Figure 6. Sample J18 observations versus model results, as in Figure 5.

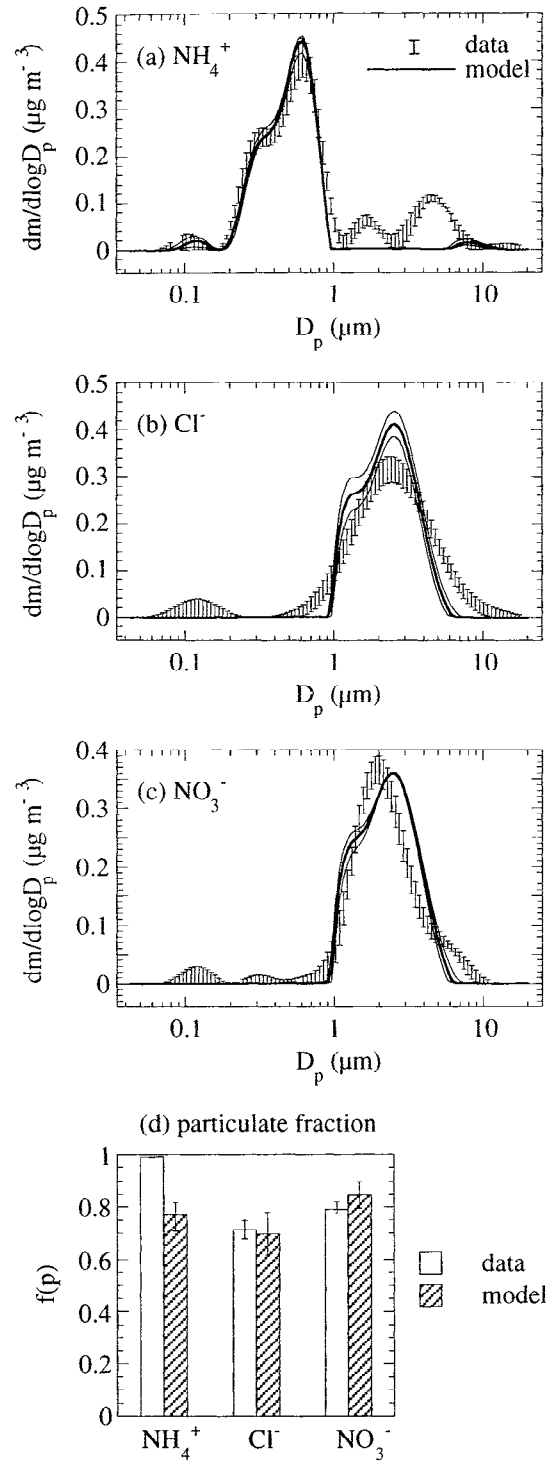

Figure 7. Sample J21 observations versus model results, as in Figure 5.

When NH_4^+ peaks were present in the coarse mode, observations indicated that they were accompanied by SO_4^{2-} peaks (Figures 3d and 3e). Since SO_4^{2-} was assumed to be fully internally mixed with the other aerosol constituents in the coarse mode, the resulting aerosol solution was neutralized by the observed sea

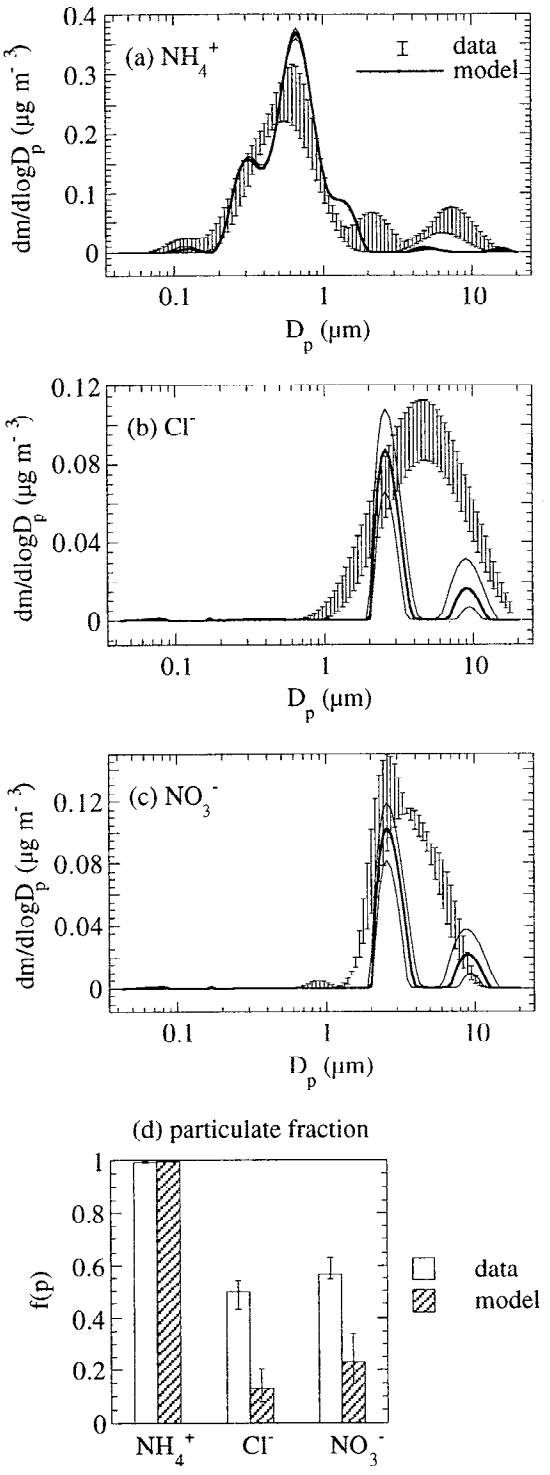

Figure 8. Sample J22 observations versus model results, as in Figure 5.

salts and demonstrated little thermodynamic demand for NH_4^+. Thus it was hypothesized that some particles in the coarse mode may have been more acidic than others, and therefore capable of attracting NH_4^+. When a mixture of separate modified sea-salt particles and organic-enriched ammonium-sulfate particles was assumed in all size bins (see section 3.2.2), predicted coarse-mode NH_4^+ more closely matched observations, and accumulation-mode predictions were unchanged (size distributions shown only for sample J22 in Figure 9a). These results suggest that it is possible that some degree of external mixture may explain the deviation between predictions and observations, but it is impossible to draw more definitive conclusions due to the lack of data on actual mixing state.

4.1.2. HCl/Cl^-. Modeled Cl^- was compared with observations for the four samples exhibiting Cl^- above detection limits. The predicted particulate fraction was within experimental uncertainty

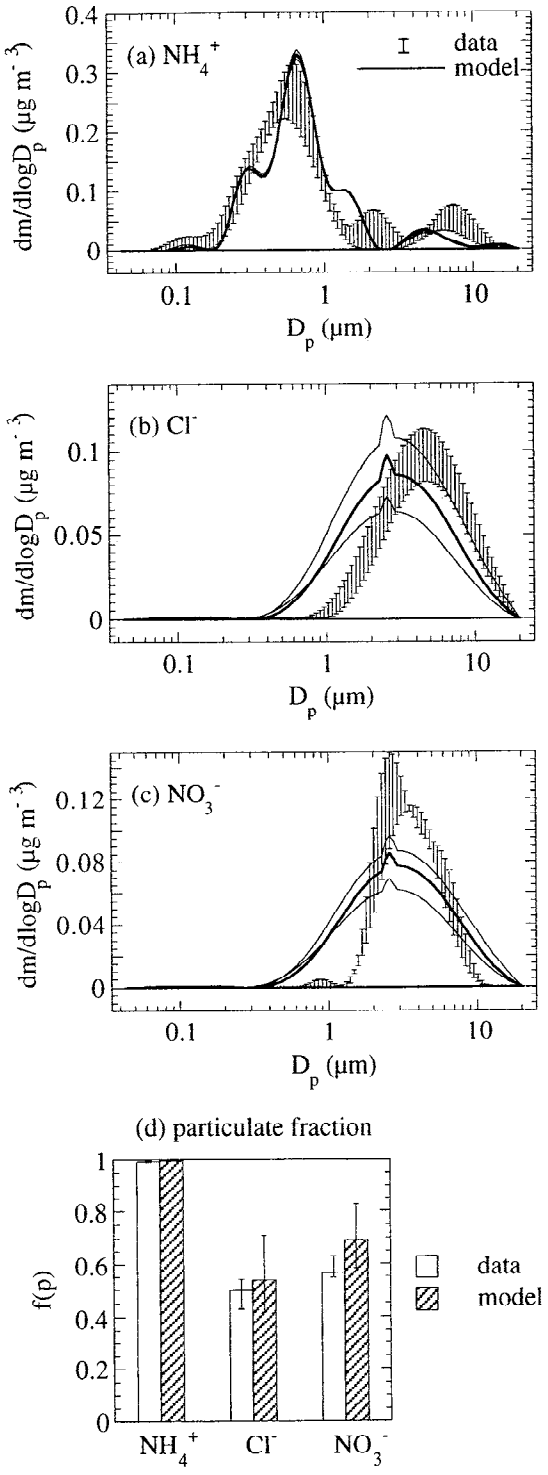

Figure 9. Sample J22 observations versus sensitivity test results, as in Figure 5, when aerosols were assumed to be separated into modified sea salt and organic-enriched ammonium-sulfate particles.

in two continentally influenced samples (Figures 5d and 7d), but the predicted and observed size distributions differed by more than experimental uncertainties in one sample in some particle size ranges (Figure 7a). In the marine sample the particulate fraction of Cl^- was overpredicted by ~10% (Figure 6d), but the shape of the predicted size distribution closely approximated the observed shape (Figure 6b). In the last, continentally influenced sample, Cl^- was severely underpredicted (Figure 8b), but the predictions were somewhat improved when separate modified sea-salt particles and organic-enriched ammonium-sulfate particles were assumed in all size bins, leaving less acidified sea salts to retain Cl^- (Figure 9b). Overall, it appeared that some aerosols may have been at or near equilibrium with HCl, but there were significant deviations between predictions and observations in some samples that could not be explained.

4.1.3. HNO_3/NO_3^-. Modeled NO_3^- was compared with observations for the four samples exhibiting NO_3^- above detection limits. As in the case of Cl^-, the predicted particulate fraction agreed with observations in two continentally influenced samples (Figures 5d and 7d), but the predicted and observed mass size distributions differed by more than experimental uncertainties in at least some size ranges (Figures 5c and 7c). By contrast, in the marine sample, the particulate fraction of NO_3^- was severely overpredicted (Figure 6d), corresponding to underprediction of HNO_3. Thermodynamically, the marine sample was capable of absorbing all available HNO_3, almost twice as much as observations indicated was actually absorbed. In that sample, NO_3^- was underpredicted in the small particles due at least in part to the underprediction of HNO_3, but overpredicted in the large particles despite underprediction of HNO_3 (Figure 6c). These deviations between observations and equilibrium model results may have been due to the actual undersaturation of large, fresh marine particles that has been previously observed in coastal environments [e.g., *Pio and Lopes,* 1998; *Roth and Okada,* 1998]. In the last, continentally influenced sample, NO_3^- was severely underpredicted (Figure 8c), but the predictions were somewhat improved when an external mixture of modified sea salts and ammonium sulfates was assumed (Figure 9c); as in the case of Cl^-, the predicted size distribution still deviated from observations, but the predicted particulate fraction lay within experimental uncertainty (Figure 9d). Overall, it appeared that some continental aerosols may have been at or near equilibrium with HNO_3 but that some coarse-mode marine aerosols were undersaturated. However, there were again significant deviations between predictions and observations in some samples that could not be explained.

4.1.4. $HCOOH/HCOO^-$ and CH_3COOH/CH_3COO^-. The gas-aerosol partitioning of formic and acetic acids was examined in the two samples for which both aerosol and gas data were available, J11 and J12. About 5–7% of the formic acid was observed in the aerosol phase in both samples (compare Tables 3 and 4), consistent with other observations of 1–10% [*Andreae et al.*, 1987; *Grosjean*, 1989; *Dibb et al.*, 1996], and ~3% of the acetic acid was observed in the aerosol phase, consistent with other observations of 0.3–20% [*Grosjean*, 1989; *Dibb et al.*, 1996]. In both samples, formate and acetate were concentrated in the submicron size range, consistent with most other observations [*Andreae et al.*, 1987; *Ludwig and Klemm*, 1988; *Matsumoto et al.*, 1998].

The model represented the temperature-dependent dissociation and volatility of both acids, but did not account for the water uptake of the dissolved species or the nonideality of their activity coefficients due to lack of thermodynamic data. Neglecting water uptake likely introduced negligible error due to the relatively low aerosol concentrations of these species [*Meng et al.*, 1995], whereas neglecting nonideality of activity coefficients may have resulted in an overestimate of the organic species in solution. However, the model predicted <0.01% of formate and <0.001% of acetate in the aerosol phase, at least two orders of magnitude less than observed.

The severe underprediction of formate and acetate indicated that the observations could not be explained by effective Henry's law partitioning of the acids to the aerosol solution. Similar results have been reported elsewhere, and it has been suggested that associated ammonium formate and ammonium acetate in solution may explain the discrepancy [*Meng et al.*, 1995, and references therein]. Since no data were available for the dissociation of $CH_3COONH_4(aq)$ and $HCOONH_4(aq)$, an estimate of 2.952×10^{-4} *M* for forward dissociation of $CH_3COONH_4(aq)$ at 25°C was used [*Meng et al.*, 1995]. When $CH_3COONH_4(aq)$ was thus included, the model predicted <0.5% of water-soluble acetate in the aerosol phase, still a factor of 6 lower than observed.

In summary, the observed gas-aerosol partitioning of formic and acetic acids could not be explained. The potential presence of $CH_3COONH_4(aq)$ did not appear to account for the discrepancy in acetic acid, but firm conclusions cannot be drawn until more accurate thermodynamic data are available. Other potential explanations include the possible presence of anhydrides in the acidic accumulation-mode aerosol solution, or the partitioning of the monocarboxylic acids to an organic surface active layer or other organic matter phase that is not well mixed with the inorganic solution [e.g., *Pankow*, 1994a, b; *Odum et al.*, 1996; *Bowman et al.*, 1997].

4.2. Impact of Nonvolatile Organic Acids on Gas-Aerosol Partitioning

The sensitivity of the above results to the presence of nonvolatile organic acids was tested as follows. Sensitivity to $CH_3SO_3^-$ was tested by removing it from the model. Unlike $CH_3SO_3^-$, the dicarboxylic acids were not included in the model thus far due to their low concentrations and the lack of complete thermodynamic data. Sensitivity to the combined presence of the three acids was thus tested by adding them. The results of the sensitivity tests were used to evaluate the influence of the organic acids on the partitioning of NH_4^+, Cl^-, and NO_3^-.

4.2.1. Impact of methanesulfonic acid. Thermodynamic data included in the model represented the 25°C dissociation, water uptake, and activity coefficients in $CH_3SO_3H(aq)$ solution [*Covington et al.*, 1973; *Clegg and Brimblecombe*, 1985]. In the marine sample (J18), predicted NH_4^+ was decreased by 27% when $CH_3SO_3^-$ was removed, but Cl^- and NO_3^- partitioning were not affected (Table 6). In the remaining samples, predicted NH_4^+ was decreased by 0–3%, whereas Cl^- and NO_3^- were increased by 0–2%. Thus $CH_3SO_3^-$ served to retain a significant fraction of aerosol NH_4^+ in the marine sample, but had a more uniform and moderate influence on gas-aerosol partitioning in the continentally influenced samples, slightly increasing uptake of NH_4^+ and slightly displacing Cl^- and NO_3^-.

4.2.2. Impact of dicarboxylic acids. Thermodynamic data included in the model represented the 25°C dissociation of oxalic, succinic, and glutaric acids [*Lide*, 1996], but did not account for their water uptake or the nonideality of their activity coefficients due to lack of data. Thus the model represented only their influence on the charge balance in each aerosol size bin. Because of the relatively low concentrations and nonvolatility of all three acids, this was considered to be adequate to first order.

Since they were present in the acidic accumulation-mode aerosols, succinic and glutaric acids were predicted to be <10% dissociated in both samples, and oxalic acid was predicted to be only ~15–30% dissociated (Table 7). However, calculations indicated that all three organics were present at nearly an order of magnitude below their solubility limit in pure water [*Saxena and Hildemann*, 1996], confirming the possibility that they remained fully dissolved in the bulk aerosol solution. The marine sample (J18) was unaffected by the presence of the acids due to their low concentrations in that sample (Table 6). In the continentally influenced samples, 0–2% of additional NH_4^+ was retained by the dissociated acids, whereas 0–6% of Cl^- and NO_3^- were displaced. These results support the possibility that dicarboxylic acids in solution may be responsible for a fraction of chloride losses from aged sea-salt aerosols and that oxalic acid may be most important [*Kerminen et al.*, 1998b] due to higher concentrations combined with a higher degree of dissociation.

5. Summary and Conclusions

The EQUISOLV II model was applied to size-resolved aerosol and gas field data gathered during EAAS in order to estimate whether gas-aerosol equilibrium was achieved during EAAS and how organic acids may have affected it. The conclusions presented above can be summarized as follows:

1. Accumulation-mode aerosols appeared to be at or near equilibrium with NH_3 in all samples.

2. Coarse-mode aerosols containing NH_4^+ did not appear to be at equilibrium with NH_3 unless some degree of external mixture were assumed, but definitive conclusions could not be drawn from this since no data were available on aerosol mixing state.

3. Coarse-mode aerosols of recent marine origin did not appear to be at equilibrium with HNO_3 but may have been closer to equilibrium with HCl. This may be explained by the lag time in equilibration with HNO_3 that has been documented in other work on coastal aerosols.

4. Coarse-mode aerosols that were continentally influenced appeared to be at or near equilibrium with HNO_3 and HCl simultaneously in some samples, but discrepancies between observations and model results could not be explained in other samples.

5. The gas-acrosol partitioning of formic and acetic acids could not be explained by effective Henry's law partitioning to the aerosol phase, consistent with the results of other studies. Furthermore, using existing indirect thermodynamic data, the differences between observed and predicted water-soluble acetate could not be explained by the potential presence of CH_3COONH_4(aq).

6. In marine aerosols, $CH_3SO_3^-$ retained ~30% of observed NH_4^+ but did not affect Cl^- and NO_3^-. In continental aerosols, $CH_3SO_3^-$ had a more uniform and moderate influence, retaining ~0–3% of NH_4^+ and displacing ~0–2% of Cl^- and NO_3^-.

Table 7. Percentage of Dicarboxylic Acids Predicted in a Dissociated Form

Sample	Oxalic	Succinic	Glutaric
J11	26.00	0.04	0.03
J12	18.55	0.29	0.52
J18	24.05	—	—
J21	—	7.12	5.74
J22	15.78	0.03	0.03

7. Dicarboxylic acids appeared to be present primarily in their fully associated form. Succinic and glutaric acids were predicted to be <10% dissociated in both samples, whereas oxalic acid was predicted to be ~15–30% dissociated. Together, the acids had no influence on the marine sample. In the continentally influenced samples, however, the acids retained ~0–2% additional NH_4^+ and displaced ~0–6% of Cl^- and NO_3^-.

Generalization of these conclusions provides insight into whether the observations fit together to form a physically consistent picture of size-resolved aerosol chemical composition and gas-aerosol interaction. Overall, a physically consistent picture was generally verified in the accumulation mode, except with respect to monocarboxylic acid partitioning. However, in the coarse mode, where aerosols were often composed of more complex mixtures of primary and secondary constituents, it was often not possible to verify such a picture. It was also not possible to identify the first-order source of error when predictions deviated from observations in the coarse mode, such as whether the aerosols were actually out of gas-aerosol equilibrium or were inadequately represented by the model. Since results in such cases were sensitive to mixing state assumptions, additional data on the actual mixing state of the coarse-mode aerosols would have provided an important model constraint. Sensitivity tests using one and two aerosol size bins showed that accurate modeling of gas-aerosol interaction is also likely to require some degree of aerosol size resolution.

Acknowledgments. M. Z. Jacobson and A. M. Fridlind were supported by the National Science Foundation through agreements ATM-9504481 and ATM-9614118 and a Graduate Student Fellowship, by the David and Lucile Packard Foundation and the Hewlett-Packard company through a Stanford University Terman Fellowship, and by the National Aeronautics and Space Administration through agreement NIP-0000-0003. V.-M. Kerminen and R. E. Hillamo were supported by the Academy of Finland through contract 46906 and by the Maj and Tor Nessling Foundation. J.-L. Jaffrezo and V. Ricard were supported by the Institut Français de Recherche et Technologie Polaire through program 323 and by CNRS-Programme National de Chémie de l'Atmosphère under action "Impact radiatif des aérosols."

References

Andreae, M. O., R. W. Talbot, and S.-M. Li, Atmospheric measurements of pyruvic and formic acid, *J. Geophys. Res.*, *92*, 6635–6641, 1987.

Bouwman, A. F., D. S. Lee, W. A. H. Asman, F. J. Dentener, K. W. Van Der Hoek, and J. G. J. Olivier, A global high-resolution emission inventory for ammonia, *Global Biogeochem. Cycles*, *11*, 561–587, 1997.

Bowman, F. M., J. R. Odum, J. H. Seinfeld, and S. N. Pandis, Mathematical model for gas-particle partitioning of secondary organic aerosols, *Atmos. Environ.*, *31*, 3921–3931, 1997.

Clegg, S. L., and P. Brimblecombe, The solubility of methanesulfonic acid and its implications for atmospheric chemistry, *Environ. Technol. Lett.*, *6*, 269–278, 1985.

Covington, A. K., R. A. Robinson, and R. Thompson, Osmotic and activity coefficients for aqueous methane sulfonic acid solutions at 25°C, *J. Chem. Eng. Data*, *18*, 422–423, 1973.

Dibb, J. E., R. W. Talbot, S. I. Whitlow, M. C. Shipham, J. Winterle, J. McConnell, and R. Bales, Biomass burning signatures in the atmosphere and snow at Summit, Greenland: An event on 5 August 1994, *Atmos. Environ.*, *30*, 553–561, 1996.

Erisman, J.-W., A. W. M. Vermetten, W. A. H. Asman, A. Waijers-Ijpelaan, and J. Slanina, Vertical distribution of gases and aerosols: The behaviour of ammonia and related components in the lower atmosphere, *Atmos. Environ.*, *22*, 1153–1160, 1988.

Grosjean, D., Organic acids in southern California air: Ambient concentrations, mobile source emissions, in situ formation and removal processes, *Environ. Sci. Technol.*, *23*, 1506–1514, 1989.

Hayami, H., and G. R. Carmichael, Analysis of aerosol composition at Cheju Island, Korea, using a two-bin gas–aerosol equilibrium model, *Atmos. Environ.*, *31*, 3429–3439, 1997.

Hayami, H., and G. R. Carmichael, Factors influencing the seasonal

variation in particulate nitrate at Cheju Island, South Korea, *Atmos. Environ., 32*, 1427–1434, 1998.

Hildemann, L. M., A. G. Russell, and G. R. Cass, Ammonia and nitric acid concentrations in equilibrium with atmospheric aerosols: Experiment vs. theory, *Atmos. Environ., 18*, 1737–1750, 1984.

Intergovernmental Panel on Climate Change, *Climate Change 1995*, edited by J. T. Houghton et al., Cambridge Univ. Press, New York, 1996.

Jacobson, M. Z., Numerical techniques to solve condensational and dissolutional growth equations when growth is coupled to reversible reactions, *Aerosol Sci. Technol., 27*, 491–498, 1997a.

Jacobson, M. Z., Development and application of a new air pollution modeling system, II, Aerosol module structure and design, *Atmos. Environ., 31*, 131–144, 1997b.

Jacobson, M. Z., Development and application of a new air pollution modeling system, part III, Aerosol-phase simulations, *Atmos. Environ., 31*, 587–608, 1997c.

Jacobson, M. Z., Studying the effects of calcium and magnesium on size-distributed nitrate and ammonium with EQUISOLV II, *Atmos. Environ., 33*, 3635–3649, 1999a.

Jacobson, M. Z., *Fundamentals of Atmospheric Modeling*, 656 pp., Cambridge Univ. Press, New York, 1999b.

Jaffrezo, J.-L., N. Calas, and M. Bouchet, Carboxylic acids measurements with ionic chromatography, *Atmos. Environ., 32*, 2705–2708, 1998.

Kawamura, K., H. Kasukabe, and L. A. Barrie, Sources and reaction pathways of dicarboxylic acids, ketoacids and dicarbonyls in Arctic aerosols: One year of observations, *Atmos. Environ., 30*, 1709–1722, 1996.

Kerminen, V.-M., R. E. Hillamo, T. Mäkelä, J.-L. Jaffrezo, and W. Maenhaut, The physicochemical structure of the Greenland summer aerosol and its relation to atmospheric processes, *J. Geophys. Res., 103*, 5661–5670, 1998a.

Kerminen, V.-M., K. Teinilä, R. Hillamo, T. Pakkanen, Substitution of chloride in sea-salt particles by inorganic and organic anions, *J. Aerosol Sci., 8*, 929–942, 1998b.

Kerminen, V.-M., K. Teinilä, R. Hillamo, and T. Mäkelä, Size-segregated chemistry of particulate dicarboxylic acids in the Arctic atmosphere, *Atmos. Environ., 33*, 2089–2100, 1999.

Lefer, B. L., R. W. Talbot, and J. W. Munger, Nitric acid and ammonia at a rural northeastern U.S. site, *J. Geophys. Res., 104*, 1645–1661, 1999.

Lide, D. R. (Ed.), *CRC Handbook of Chemistry and Physics*, CRC Press, Boca Raton, Fla., 1996.

Ludwig, J., and O. Klemm, Organic acids in different size classes of atmospheric particulate material, *Tellus, Ser. B, 40*, 340–347, 1988.

Maenhaut, W., R. Hillamo, T. Mäkelä, J.-L. Jaffrezo, M. H. Bergin, and C. I. Davidson, A new cascade impactor for aerosol sampling with subsequent PIXE analysis, *Nucl. Instrum. Methods Phys. Res. B, 109/110*, 482–487, 1996.

Matsumoto, K., I. Nagao, H. Tanaka, H. Miyaji, T. Iida, and Y. Ikebe, Seasonal characteristics of organic and inorganic species and their size distributions over the northwest Pacific Ocean, *Atmos. Environ., 32*, 1931–1946, 1998.

Meng, Z., and J. H. Seinfeld, Time scales to achieve atmospheric gas-aerosol equilibrium for volatile species, *Atmos. Environ., 30*, 2889–2900, 1996.

Meng, Z., J. H. Seinfeld, and P. Saxena, Gas/aerosol distribution of formic and acetic acids, *Aerosol Sci. Technol., 23*, 561–578, 1995.

Meng, Z., D. Dabdub, and J. H. Seinfeld, Size-resolved and chemically resolved model of atmospheric aerosol dynamics, *J. Geophys. Res., 103*, 3419–3435, 1998.

Odum, J. R., T. Hoffmann, F. Bowman, D. Collins, R. C. Flagan, and J. H. Seinfeld, Gas/particle partitioning and secondary organic aerosol yields, *Environ. Sci. Technol., 30*, 2580–2585, 1996.

Pankow, J. F., An absorption model of gas/particle partitioning of organic compounds in the atmosphere, *Atmos. Environ., 28*, 185–188, 1994a.

Pankow, J. F., An absorption model of the gas/aerosol partitioning involved in the formation of secondary organic aerosol, *Atmos. Environ., 28*, 189–193, 1994b.

Pio, C. A., and D. A. Lopes, Chlorine loss from marine aerosol in a coastal atmosphere, *J. Geophys. Res., 103*, 25,263–25,272, 1998.

Roth, B., and K. Okada, On the modification of sea-salt particles in the coastal atmosphere, *Atmos. Environ., 32*, 1555–1569, 1998.

Saxena, P., and L. M. Hildemann, Water-soluble organics in atmospheric particles: A critical review of the literature and application of thermodynamics to identify candidate compounds, *J. Atmos. Chem., 24*, 57–109, 1996.

Sirois, A., and L. A. Barrie, Arctic lower tropospheric aerosol trends and composition at Alert, Canada: 1980–1995, *J. Geophys. Res., 104*, 11,599–11,618, 1999.

Stumm, W., and J. J. Morgan, *Aquatic Chemistry*, 1022 pp., John Wiley, New York, 1996.

Talbot, R. W., A. S. Vijgen, and R. C. Harriss, Soluble species in the Arctic summer troposphere: Acidic gases, aerosols, and precipitation, *J. Geophys. Res., 97*, 16,531–16,543, 1992.

Talbot, R. W., E. M. Scheuer, B. L. Lefer, and W. T. Luke, Measurements of sulfur dioxide during GASIE with the mist chamber technique, *J. Geophys. Res., 102*, 16,273–16,278, 1997.

Tuovinen, J.-P., T. Laurila, H. Lättilä, A. Ryaboshapko, P. Brukhanov, and S. Korolev, Impact of the sulphur dioxide sources in the Kola Peninsula on air quality in northernmost Europe, *Atmos. Environ., 27*, 1379–1395, 1993.

Virkkula, A., M. Mäkinen, R. E. Hillamo, and A. Stohl, Atmospheric aerosol in the Finnish Arctic: Particle number concentrations, chemical characteristics, and source analysis, *Water Air Soil Pollut., 85*, 1997–2002, 1995.

Virkkula, A., R. E. Hillamo, V.-M. Kerminen, and A. Stohl, The influence of Kola Peninsula, continental European and marine sources on the number concentrations and scattering coefficients of the atmospheric acrosol in Finnish Lapland, *Boreal Environ. Res., 2*, 317–336, 1997.

Virkkula, A., M. Aurela, R. Hillamo, T. Mäkelä, T. Pakkanen, V.-M. Kerminen, W. Maenhaut, F. François, and J. Cafmayer, Chemical composition of atmospheric acrosol in the European subarctic: Contributions of the Kola Peninsula smelter areas, central Europe, and the Arctic Ocean, *J. Geophys. Res., 104*, 23,681–23,696, 1999.

Voisin, D., M. Legrand, and N. Chaumerliac, Scavenging of acidic gases (HCOOH, CH_3COOH, HNO_3, HCl, and SO_2) and ammonia in mixed liquid-solid water clouds at the Puy de Dôme mountain (France) , *J. Geophys. Res., 105*, 6817–6835, 2000.

Wexler, A. S., and J. H. Seinfeld, The distribution of ammonium salts among a size and composition dispersed aerosol, *Atmos. Environ., Part A, 24*, 1231–1246, 1990.

Wolfenbarger, J. K., and J. H. Seinfeld, Inversion of aerosol size distribution data, *J. Aerosol Sci., 21*, 227–247, 1990.

Zhang, X., and P. H. McMurry, Evaporative losses of fine particulate nitrates during sampling, *Atmos. Environ., Part A, 26*, 3305–3312, 1992.

A. M. Fridlind and M. Z. Jacobson, Department of Civil and Environmental Engineering, Stanford University, Stanford, CA 94305-4020. (fridlind@stanford.edu; jacobson@ce.stanford.edu)

R. E. Hillamo and V.-M. Kerminen, Air Quality Research, Finnish Meteorological Institute, Sahaajankatu 20 E, FIN-00810 Helsinki, Finland. (Risto.Hillamo@fmi.fi; Veli-Matti.Kerminen@fmi.fi)

J.-L. Jaffrezo and V. Ricard, Laboratoire de Glaciologie et Géophysique de l'Environnement, Domaine Universitaire, Rue Molière, BP 96, 38 402 Saint Martin d'Hères Cedex, France. (jlj@glaciog.ujf-grenoble.fr; ricard@glaciog.ujf-grenoble.fr)

(Received February 15, 2000; revised April 20, 2000;
accepted April 26, 2000.)